A Melting Rate and Temperature Distribution Model for Shielded Metal Arc Welding Electrodes

The model helps in the development of weld schedules that can avoid premature electrode covering reactions

BY T. P. QUINN, A. Q. BRACARENSE and S. LIU

ABSTRACT. A mathematical model of the shielded metal arc electrode has been developed to predict its temperature distribution and melting rates. The heat transfer equations of the melting electrode were solved: Conduction along the electrode, heat delivered to the end of the solid electrode from the melt, the heat of decomposition of calcium carbonate in the covering and Joule heat generation in the electrode were considered. The thermal properties of the core rod were allowed to vary with temperature. The covering was modeled as a thermal mass (constant heat capacity) with the same temperature distribution as the core rod. The rate of heat transfer from the melt was set proportional to the current with the constant of proportionality determined by matching model predictions of the melting rate to experimental results. A finite difference technique was used to solve the final set of nonlinear equations. Experiments were conducted on E7018, 354-mm-long, 3.2-mm-diameter commercial electrodes to determine melting rates and, using thermocouples, temperature profiles. The model was able to predict the consumed length within 11 mm for currents ranging from 117.5 to 160 A. At the recommended welding current of 130 A, the rms difference in the predicted temperature between the model and experiment was 26°C (79°F). At the extremes of the range in current for practical welding, 110 and 150 A, the rms differences between the model and the experiments were 108°C (226°F) and 150 °C (302°F), respectively. The model predicted that at 130 A, the $CaCO_3$ in the covering starts to be prematurely consumed when the arc reaches the position of about 170 mm from the holder; at 140 mm from the holder, all of the $CaCO_3$ is predicted to be consumed prematurely.

T. P. QUINN is with the National Institute of Standards and Technology, Boulder, Colo., A. Q. BRACARENSE is with the Universidade Federal de Minas Gerais, Brazil, and S. LIU is with the Colorado School of Mines, Golden, Colo.

Introduction

This paper presents a model that predicts the melting rates, temperature distribution, and reactions in the covering for a shielded metal arc welding (SMAW) electrode. In SMAW a voltage is applied to a solid metal core rod and an arc is created between the wire and the base metal. The core rod is covered and part of the covering is decomposed by the heat of the arc, which provides a gas to shield the molten metal; the covering also modifies the metallurgy of the solidified weld by adding alloys, deoxidizers, fluxing agents, etc., to the weld pool (Ref. 1).

During welding, the electrode temperature rises because of internal Joule heat generation and because heat is transferred to the electrode from the arc through the melt at the end of the electrode. If the temperature of the electrode becomes too high, the covering can decompose prematurely; this adversely affects the final metallurgy of the weld and can change the melting rate and transfer mode (droplet size) (Refs. 2–5).

KEY WORDS

SMAW
E7018 Electrodes
Melting Rates
Temperature Distribution
Calcium Carbonate

Waszink and Piena (Ref. 6) developed a model to predict melting rate of SMAW electrodes. They used a heat balance between the molten tip and the closest solid part of the electrode to predict the melting rate. They concluded that the heat flow to the solid wire through the liquid tip of the electrode was dominated by convection that resulted from the electromagnetically induced flow in the pendant droplet. They also calculated that the temperature difference through the covering thickness (transverse to the length of the electrode) was from 28°C (82°F) to 78°C (172°F). Their model did not consider Joule heating or heat conduction in the core rod, and, therefore, was not able to predict the temperature distribution in the electrode away from the melting boundary.

In the model presented here, Joule heating and heat conduction were included in order to predict the temperature distribution along the electrode. The covering was modeled as a reactive thermal mass and the variation of the thermophysical properties of the core rod with temperature was considered. The position of the end of the electrode (the moving boundary) was also calculated. The resulting set of coupled nonlinear, partial differential equations was solved numerically. The model was validated through experiments on E7018 electrodes welded from 110 to 150 A.

The Model

The development of this model closely follows the derivation for the electrode extension model in gas metal arc welding (Ref. 7). Here, no heat is assumed to transfer to the environment through the covering (Fig. 1); however, heat loss due to decomposition of covering ingredients is considered. For a mild steel rod, the electrical conductivity is

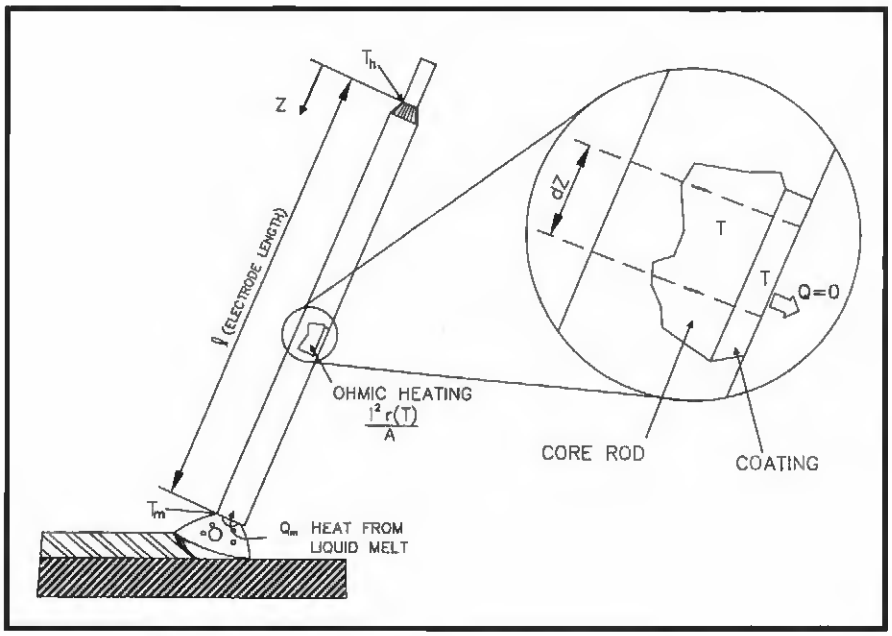

Fig. 1 — The model coordinate system and assumptions. Heat is inputted to the core rod from the melt and Joule heating. The covering is assumed to be at the same temperature as the core rod and no heat is assumed to be lost to the environment through the covering.

two orders of magnitude greater than for the covering (Ref. 6); therefore, no electrical conduction was considered in the covering. Because of the relatively small transverse temperature variation, the covering is modeled as a thermal mass with the same temperature as the core rod — Fig. 1. The heat transferred through the melt at the end of the electrode is taken as proportional to the current (Ref. 6). The constant of proportionality must be found experimentally.

The one-dimensional governing equation for the rate of heat transfer in the electrode is then given by

$$\frac{\partial}{\partial Z}\left[K(T)\frac{\partial T}{\partial Z}\right]+\frac{I^2(t)\cdot r(T)}{A^2}=$$

$$\frac{\partial T}{\partial t}\left[c(T)\cdot\rho(T)\cdot\rho_c(T)c_c(T)\frac{A_c}{A}\right]+Q_r, \quad (1)$$

where T is temperature, t is time, Z is the longitudinal coordinate (Fig. 1), K is the thermal conductivity, I is current, r is resistivity, A is cross-sectional area of the core rod, c is specific heat and ρ is density. The subscript c refers to the covering; variables without subscript are associated with the core rod. The thermophysical properties are allowed to vary with temperature.

The only reaction considered for the E7018 electrode (Table 1) was the decomposition of calcium carbonate,

Table 1 — Nominal Covering Content for the E7018 Electrode (Mild Steel Core Rod) from Ref. 8

Ingredient	Mass %
$CaCO_3$	20
CaF_2	20
TiO_2	4
Fe powder	24
Fe-Si	8
Fe-Mn	10
Clay	2
Potassium silicate	12

$CaCO_3 \rightarrow CaO+CO_2$ which is endothermic. Therefore,

$$Q_r = \Delta H(T)\, f\, \rho_{CaCO_3}\frac{A_c}{A}\frac{d\alpha_{CaCO_3}}{dt}, \quad (2)$$

where ΔH is the molar enthalpy of the reaction, f is the fraction of $CaCO_3$ in the covering, ρ_{CaCO_3} is the molar density of the $CaCO_3$, and α_{CaCO_3} is the fraction of the $CaCO_3$ reacted. ΔH is calculated from tables and adjusted to the temperature of the reactant as described in Ref. 9. The reaction rate was modeled using a topochemical contracting sphere model (Ref. 10):

$$\frac{d\alpha_{CaCO_3}}{dt}=3A_f\, e^{-\frac{E}{RT}}\left(1-\alpha_{CaCO_3}\right)^{\frac{2}{3}}, \quad (3)$$

where A_f and E are the frequency factor and activation energy for the Arrhenius equation, respectively, and R is the gas constant.

The boundary conditions for Equation 1 were

$$T(Z=0) = T_h$$
$$T(Z=\ell(t)) = T_m \quad (4)$$

where T_h is the temperature of the holder, T_m is the melting temperature and l is the length of the electrode. An additional condition, the energy balance at the tip of the core rod, is necessary because of the moving boundary:

$$-K(T)\frac{\partial T}{\partial Z}+\frac{Q_m(t)}{A}=-\rho(T)L\frac{dl}{dt}. \quad (5)$$

Q_m is the rate of heat transfer from the melt to the core rod and L is the latent enthalpy of melting of the core rod. Waszink and Piena (Ref. 6) found a linear dependence of Q_m on current:

$$Q_m = \psi\, I, \quad (6)$$

where ψ determines the melting rate of the electrode and must be found experimentally.

The equations were made dimensionless and then solved using a finite difference method (see Appendix). The thermal property data used in the model for the core rod were approximated by using the data for pure iron (Refs. 11–14). No $\rho_c c_c$ data exist for the covering of a E7018 electrode, but its covering composition is essentially bracketed by the compositions of E7016 and E7024 electrodes (Ref. 15). Waszink and Piena (Ref. 6) measured $\rho_c c_c$ for E7016 and E7024 and found them to be 2.0 and 1.9 ± 0.2 J/(cm³·K), respectively. For the model, $\rho_c c_c$ was set to 2.0 J/(cm³·K) throughout the temperature range.

Equations 1, 2 and 4–6 were first solved without considering any reaction in the covering; $Q_r = 0$. The resulting nodal temperature profiles as functions of time were fit with cubics. By solving Equation 3 using the cubic temperature profile, $d\alpha_{CaCO_3}/dt$ is found. Equations 1, 2 and 4–6 are then solved again using the calculated $d\alpha_{CaCO_3}/dt$. If the resulting temperature profile varies from the profile calculated with $Q_r = 0$ then the process can be repeated until the solution converges.

Methods

The melting rates of E7018 commercial electrodes, which were initially 354 mm long, were estimated for cur-

rents of 117, 127, 145 and 160 A. The core rod of the electrodes was 3.2 mm (⅛ in.) in diameter; the covering outside diameter was 5.6 mm. With the electrode negative, manual welds were made. The voltage was maintained at approximately 27 V with a travel speed ranging from 1.7 mm/s for 117 A to 3 mm/s for 160 A. Several electrodes were deposited bead-on-plate for each current on A36 steel plates in the flat position. After about 10, 20, 25, 30, 35, 40, 45, 50, 55, 60 or 65 s (if enough electrode remained), the welding was stopped and the remaining length of the electrode was measured. The electrode was then discarded and a new electrode was used in the next experiment.

The mean squared error between the model-predicted consumed length (no reactions in the covering considered) and the experimentally determined consumed length was minimized across the four currents by varying ψ between 2.25 and 2.70 V in increments of 0.06 V. The value ψ_{min} of ψ, which gave the minimum error, was then used to make the temperature distribution predictions. The standard deviation of ψ was determined using the bootstrap technique using 1000 resampled data sets (Ref. 16).

In the experimental temperature measurements, type K thermocouples were placed in holes of 1 mm diameter, drilled through the covering to the centerline of the rod. A set of electrodes was prepared by placing thermocouples at 25 mm intervals starting 120 mm from the tips of the electrodes. One thermocouple was used per electrode. The thermocouples measured the temperature to 2% and were digitally recorded at sampling rates of at least 10/s. Sets of electrodes were welded at currents of 110, 130 and 150 A. The recommended current for this electrode is 130 A; 110 and 150 A represent the extremes of the range for which welding with this electrode is practical.

Results

Using thermophysical property data for pure iron (Refs. 11–14) and not considering the reaction in the covering, the model was fitted to the data for the consumed length tests using the commercial electrode. The model predicted the consumed length of the electrode to an rms difference of 11 mm of the experimental data (Fig. 2); ψ_{min} = 2.44 V. ψ_{min} was determined to a standard deviation of 0.02 V. This compares with values of 2.8–5.4 V for ψ found by Waszink and Piena (Ref. 6). As the current is increased, the melting rate increases — Fig. 2. This is due to the temperature increase in the electrode away from the arc.

The spatial temperature profile predicted by the model starts at the temperature of the holder, climbs gradually, and then remains relatively flat before rising sharply to the melting temperature at the end of the electrode — Fig. 3. The predicted temporal profile of temperature at a given point along the electrode rises approximately as a cubic until reached by the arc — Fig. 4. The temperature then rises rapidly. Because of the flat portion of the spatial temperature profile, each point of the electrode away from the arc is at approximately the same temperature at any given time — Figs. 4, 5. Therefore, a single cubic can be used to describe the spatial temperature profile away from the arc (that is, before the thermal shock) for each point along the electrode — Fig. 4.

Using the fitted cubic, the temperature profile was recalculated, this time considering the heat of reaction for the $CaCO_3$. For $CaCO_3$ particles of 0.075 mm diameter (200 mesh), E and A_f have been estimated as 1.80×10^5 J/mol and 1.0×10^8 1/s, respectively (Ref. 10); these values for E and A_f are used here for the $CaCO_3$ particles in the commercial electrode, which range from 0.075 mm in diameter (200 mesh) to 0.038 mm in diameter (400 mesh). The covering was assumed to be 20% $CaCO_3$. The corrected temperature profile (reaction considered) starts to differ

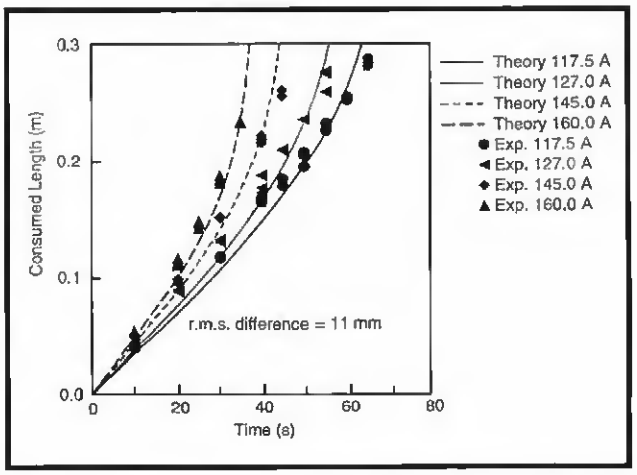

Fig. 2 — The experimental consumed length compared to the model-predicted consumed length. The model predicts that the melting rate increases (is not linear) as the electrode is consumed.

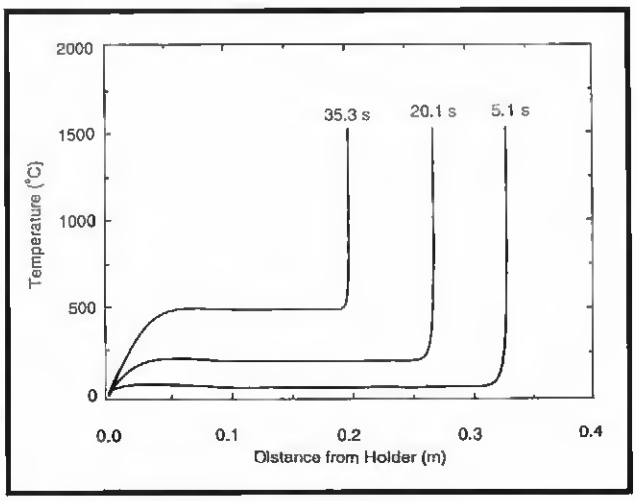

Fig. 3 — The temperature distribution predicted by the model after welding for 5.1, 20.1 and 35.3 s at 130 A with a 3.2 mm, E7018 electrode that was originally 354 mm long. The temperature distribution remains relatively flat with a rapid rise near the arc.

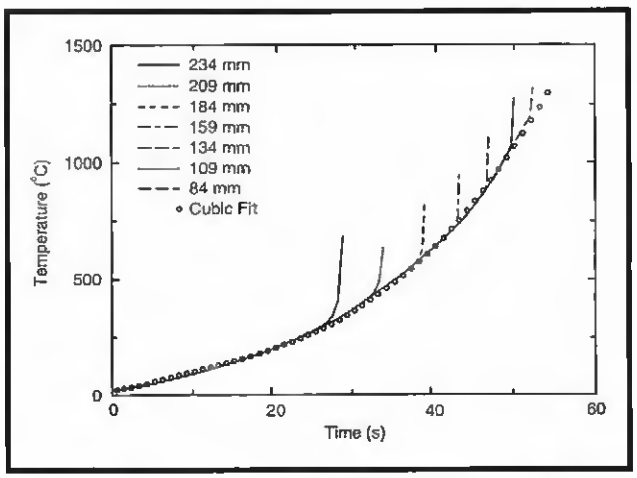

Fig. 4 — The model predicted temperature profiles at specific distances from the holder. The model predicts that all points on the electrode are at the same temperature except those close to the arc. The temperature rise away from the arc can be fit with a cubic.

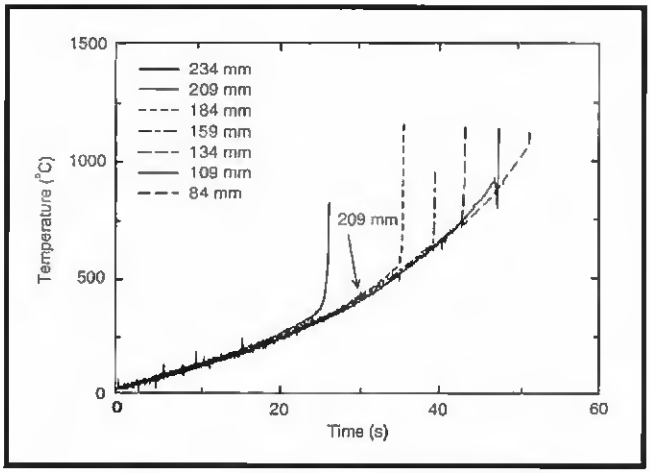

Fig. 5 — The experimentally measured temperature profiles at specific distances from the holder welded at 130 A. The measurements confirm the model prediction that all points on the electrode are at approximately the same temperature except those close to the arc.

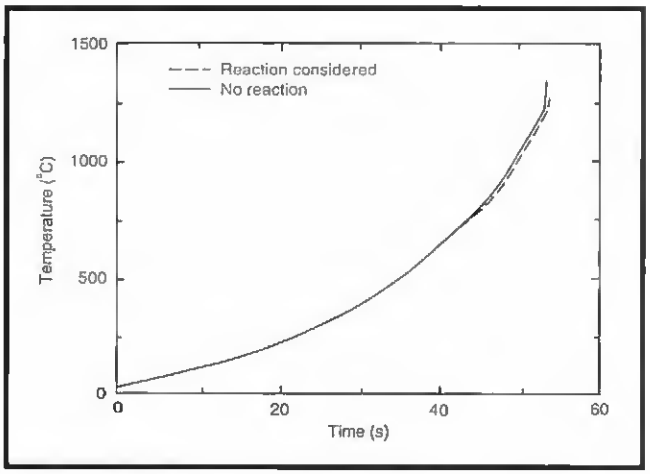

Fig. 6 — The model-predicted temperature profiles with and without considering the decomposition of the $CaCO_3$ at a point 84 mm from the holder; the current is 130 A. The reaction lowers the temperature of the electrode by a maximum of 29°C.

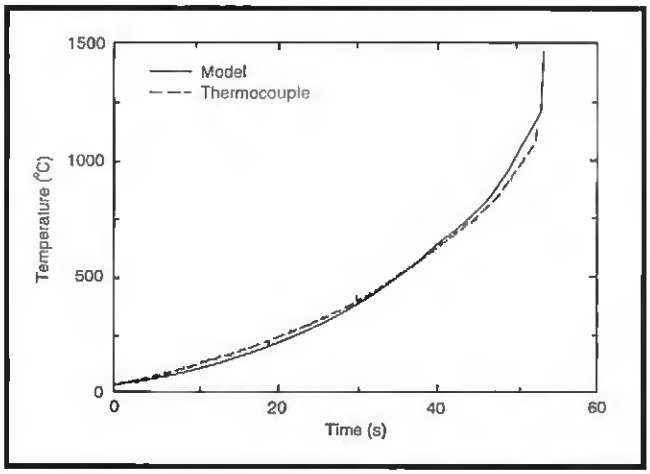

Fig. 7 — The model-predicted temperature profile compared to the experimental temperature profile at a point 84 mm from the holder welded at 130 A. The decomposition of $CaCO_3$ is considered in the model. The rms difference between the model and experiment is 26°C.

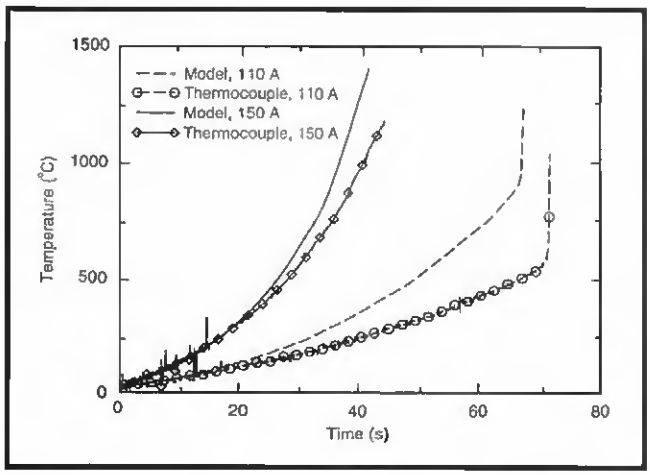

Fig. 8 — The model-predicted temperature profile compared to the experimental temperature profile at a point 84 mm from the holder welded at 110 and 150 A. The decomposition of $CaCO_3$ is considered in the model. The rms differences between the model and experiment are 108° and 158°C at 150 and 110 A, respectively.

from the temperature profile without the reaction being considered at about 750°C (1382°F) and continues at a lower temperature (Fig. 6). When this corrected temperature profile is fitted with another cubic and the equations solved again, the resulting second iteration temperature profile differs from the first iteration temperature profile by less than 3°C (35°F).

Because each point of the electrode away from the arc and the holder is at about the same temperature, the accuracy of the model can be assessed by looking at the thermocouple data farthest from the tip. At the recommended welding current of 130 A and a distance of 84 mm from the holder (234 mm from the tip), the rms difference between the model-predicted temperature profile and the temperature measured with the thermocouple is 26°C (47°F) — Fig. 7. Data used for the comparison are taken at 1-s intervals up to the region of the thermal shock. Using the same comparison format, the rms differences at the extremes of the possible currents are 108°C (194°F) at 150 A and 158°C (284°F) at 110 A — Fig. 8.

The model predicts that near the holder the $CaCO_3$ is partially or totally consumed before it reaches the arc throughout the range of practical currents — Fig. 9A–C. The lower the current, the less $CaCO_3$ consumed. At the recommended welding current, the model predicts that the $CaCO_3$ starts to be prematurely consumed at approximately 170 mm from the holder; at 140 mm from the holder (40% of the electrode) all of the $CaCO_3$ is predicted to be consumed prematurely.

Discussion

The model overpredicts the temperature at the extremes of the welding range. At 110 A, the metal transfer mechanism is primarily short circuiting (as defined in Ref. 17), which causes a different (smaller) amount of heat to be transferred from the melt to the core rod than at higher currents. The melting rate is therefore overpredicted at 110 A (Fig. 8). The convection mechanism, described in Ref. 6, that transfers heat from the melt at the end of the core rod to the core rod may be disrupted by the short circuit event. A lower rate of heat transfer from the melt would account for an overprediction in the melting rate. At 150 A, unmodeled reactions in the cover-

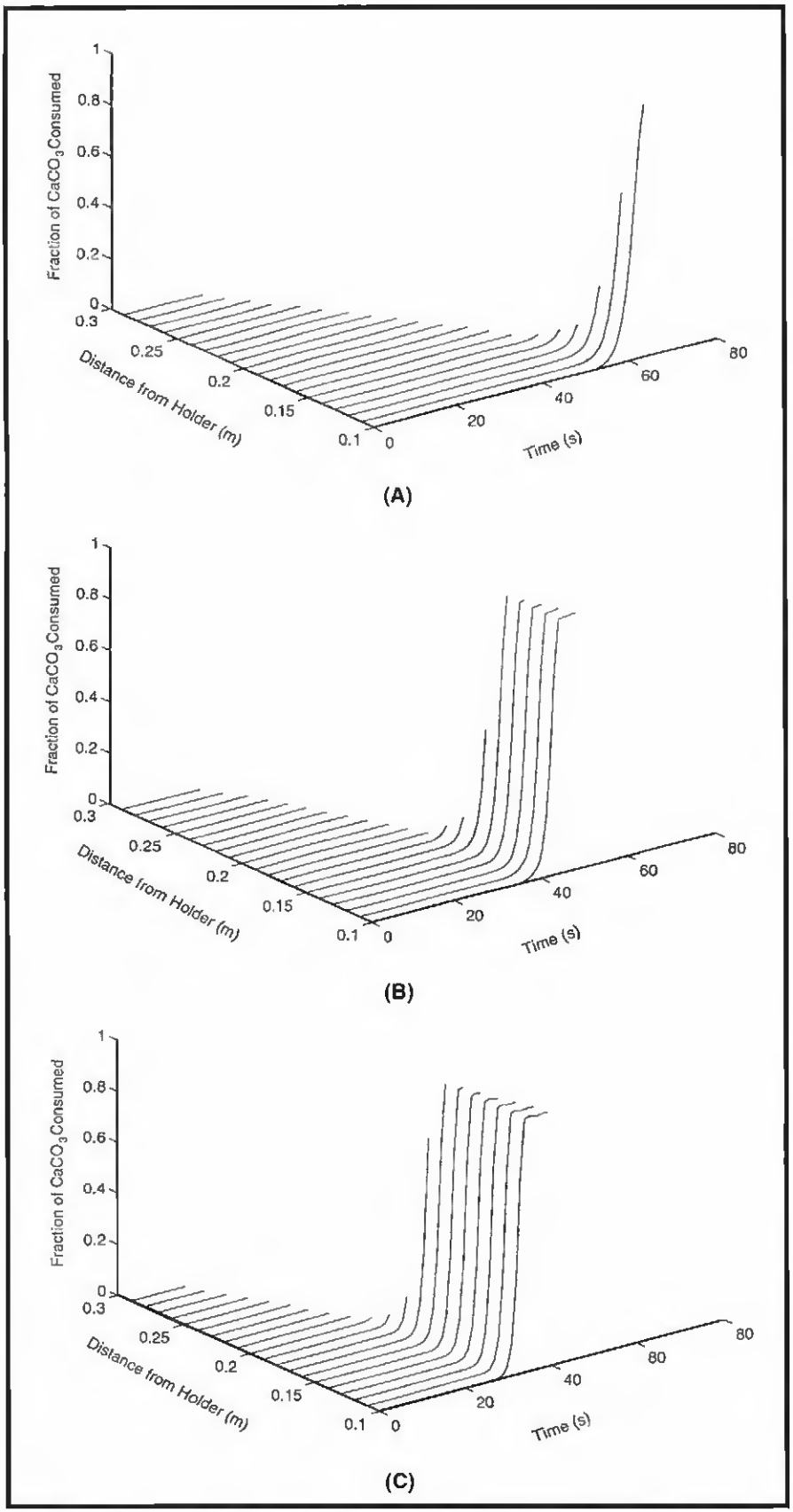

Fig. 9 — The fraction of the $CaCO_3$ that the model predicts reacted (before reached by the arc) welded at A — 110 A; B — 130 A; or C — 150 A. Some of the $CaCO_3$ reacts before it reaches the arc even for low welding currents. At the recommended welding current of 130 A, the model predicts that all of the $CaCO_3$ in the remaining electrode has been consumed when there is 40% of the electrode remaining.

ing may cause some of the difference found between the experiments and model.

The model assumes that no heat is lost to the environment from the covering. To understand the error introduced by this assumption, the heat lost to the environment was estimated and compared to the heat terms considered in the model for a 1-mm section of the remaining electrode welded at 130 A after 25 s of welding — Fig. 10. The 1-mm section was taken at the center of the remaining electrode. The electrode was modeled as a black body for the radiation term and as a vertical cylinder with natural convection flow of air for the convection term (Ref. 18). The temperature of the cylinder was taken as the temperature of the flat portion of the electrode — Fig. 3. The sum of the absolute values of the heat for the convection and radiation is 4% of the sum of the absolute values of the heat storage, generation and reaction terms. After 35 s, this fraction rises to 6%. The largest heating component that is not modeled is radiation. In this region of the electrode, the generation and heat storage terms dominate the environmental losses; close to the arc, the conduction term dominates because of the large thermal gradient. The heat lost to the reaction of the $CaCO_3$ is also small — Fig. 6.

X-ray diffraction analysis of the covering of an E7018 electrode (Ref. 19) also predicts that the $CaCO_3$ in the covering is reacting before it reaches the arc. A direct comparison of the results is difficult because of the difference in the size of the electrodes used in the two studies and the relative nature of the X-ray diffraction analysis of the composition of the covering.

There is a large range of values for A_f and E in the literature. In Ref. 10, A_f can range from $10^{12.2}$ to $10^{6.1}$ s^{-1} depending on the type of experiment used to determine the constant. Here we used A_f taken from an experiment using an N_2 atmosphere, but the increase in temperature of the sample was slower than that experienced by the electrode (30°C (54°F) vs. 200°C (360°F)/min). Better predictions of the covering reactions can be made if A_f and E are determined for heating regimes and atmospheres seen by the electrodes.

The model predictions indicate that the amount (mass) of some covering ingredients ($CaCO_3$ for E7018) that reach the arc will vary depending on their position relative to the holder and on the length of the electrode. Therefore, it is likely there will be a variation in the composition and/or microstructure of the deposited weldment (Ref. 2). The model can be used by those who are designing

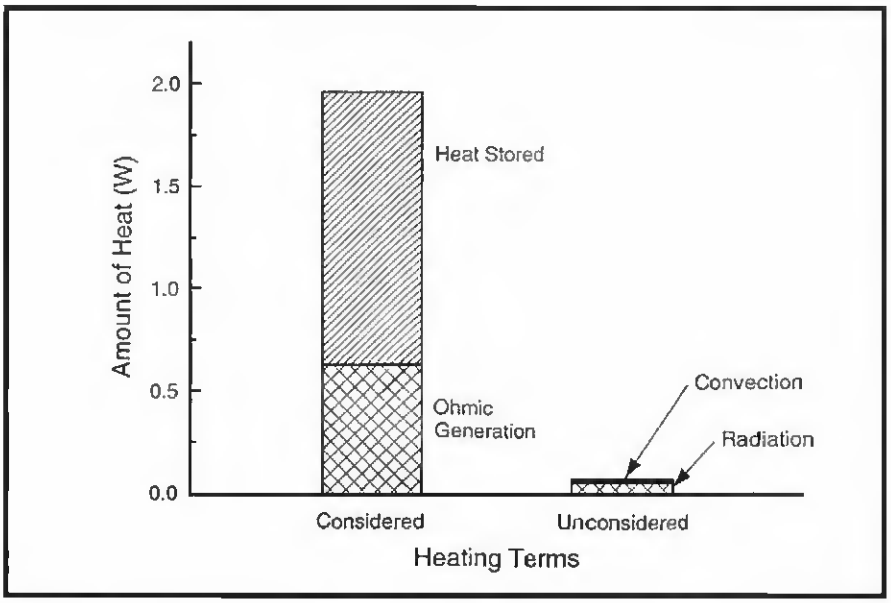

Fig. 10 — The heating terms considered in the model and the heat lost to the environment for a 1-mm section of the remaining electrode welded at 130 A after 25 s of welding. The 1-mm section is at the center of the remaining electrode.

covering compositions and by those who are designing weld schedules for existing electrodes to avoid these possible variations. For those designing weld schedules, the length of the electrode that can be used in a single pass without degradation in the covering for a given current can be predicted. For those designing coverings, the amount of a given ingredient that will reach the arc can be predicted.

Conclusions

1) A model that predicts melting rate, electrode temperature, and covering reactions for SMAW has been developed. For the E7018 electrode used in the study, the model was able to predict the consumed length to 11 mm. At the recommended welding current of the experimental electrode (130 A), the rms difference in the predicted temperature between the model and experiment is 26°C. At the extremes of the current range for practical welding, 110 and 150 A, the rms difference between the model and the experiments was 108°C and 150°C.

2) The model can be used to design weld schedules to avoid premature covering reactions, or it can be used to select covering ingredients for a particular weld schedule. For example, the model predicts that, at the recommended welding current of 130 A for the 3.2-mm-diameter, 354-mm-long, E7018 electrode considered here, the $CaCO_3$ in the covering starts to be prematurely consumed at approximately 170 mm from the holder; at 140 mm from the holder all of the $CaCO_3$ is predicted to be consumed prematurely.

Nomenclature

A Cross-sectional area of the core rod

A_i Frequency factor for the Arrhenius equation

A_c Cross-sectional area of the covering

$c(T)$ Specific heat of the core rod

$$B(u)=\frac{A_c\rho_c c_c\left(u\left[T_m-T_h\right]+T_h\right)}{AK\left(u\left[T_m-T_h\right]+T_h\right)}$$

Thermal storage term for the covering

$$B(u)=\frac{A_c\rho_c c_c\left(u\left[T_m-T_h\right]+T_h\right)}{AK\left(u\left[T_m-T_h\right]+T_h\right)}$$

Dimensionless thermal storage term for the covering

$$C(u)=1/\alpha\left(u\left[T_m-T_h\right]+T_h\right)$$

Reciprocal of thermal diffusivity

$$C(u)=1/\alpha\left(u\left[T_m-T_h\right]+T_h\right)$$

Dimensionless reciprocal of thermal diffusivity

E The activation energy for the Arrhenius equation

f Fraction of $CaCO_3$ in the covering before any reactions

$$F=\frac{\psi^2}{K(T_m)r(T_m)(T_m-T_h)}$$

Multiplying factor used for convenience

ΔH Molar enthalpy of the calcium carbonate reaction

I Welding current

$K(T)$ Thermal conductivity

ℓ Electrode length, Fig. 1

ℓ_0 Electrode length at t = 0

L Specific enthalpy

$$q_j=\frac{I^2\ell_0^2 r(T_m)}{A^2K(T_m)(T_m-T_h)}$$

Dimensionless, volumetric, Joule heat generation

Q_m Rate of heat transfer to solid core rod from the melt ($z=\ell$)

Q_r Rate of heat used by the calcium carbonate reaction

$r(T)$ Resistivity of core rod

$$r^*(u)=\frac{r\left(T\left[T_m-T_h\right]+T_h\right)}{r(T_m)}$$

Dimensionless resistivity

R The universal gas constant

$s(t)=\ell(t)/\ell_0$ Dimensionless electrode length

t Time

T Temperature of core rod; subscripts h and m refer to T at $Z=0$ (holder) and $Z=\ell$ (melting). Subscript 0 refers to T at $t=0$.

$$u=\frac{T-T_h}{T_m-T_h}$$

Dimensionless temperature

$$v=\int_0^u K\left(\zeta\cdot\left[T_m-T_h\right]+T_h\right)d\zeta$$

Transformed temperature

v_m v at $u=1$ (melting)

$x=Z/\ell_0$ Dimensionless coordinate

Z Spatial coordinate, Fig. 1

Greek

$\alpha(T)$ Thermal diffusivity $=\dfrac{K}{\rho c}$

α_{CaCO_3} The fraction of $CaCO_3$ reacted

$$\lambda = \frac{L}{C(u=1)(T_m - T_h)}$$

Second Kutateladze number

$$\xi = \frac{x}{s(\tau)}$$ Transformed coordinate

$\rho(T)$ Density of core rod

ρ_{CaCO_3} Molar density of Calcium Carbonate

$$\tau = \frac{t\alpha(T_m)}{\ell_0^2}$$ Fourier number

Subscripts

c	Refers to covering
no subscript	Refers to core rod

Appendix

Equation 1 can be made dimensionless in the form of

$$\frac{\partial^2 v(u)}{\partial x^2} + q_j\, r^*(u) = \left(C^*[u] + B^*[u]\right)\frac{\partial v(u)}{\partial \tau} \qquad \text{(A1)}$$

with dimensionless boundary conditions

$$v(x=0,\tau)=0,$$
$$v(x=s[\tau],\tau)=v_m,$$
$$\left.\frac{\partial v}{\partial x}\right|_{x=s} - \left(F q_j\right)^{1/2} = \lambda\frac{ds}{d\tau}, \qquad \text{(A2)}$$

and dimensionless initial conditions

$$s(\tau=0)=1,$$
$$v(x,\tau=0)=v_0(x). \qquad \text{(A3)}$$

The transient problem is solved as in Ref. 7: Equations A1–A3 are solved by using the coordinate transformation

$$\xi(\tau) = \frac{x}{s(\tau)} \qquad \text{(A4)}$$

to fix the moving boundary according to Ref. 19. The resulting nonlinear partial differential equation is solved by using central differences in ξ for unequally spaced nodes (Ref. 20). The nodes are spaced in a geometric progression with more nodes near the $\xi = 1$ boundary. A backward differentiation method for stiff equations is used to solve the resulting set of ordinary differential equations.

As in Ref. 7, $K(T)$ is first smoothed from room temperature to the melting point using a moving average to avoid step changes in $K(T)$ when the material changes from one solid phase to another; a piecewise cubic spline is then fit to the tabulated $K(T)$ and integrated to get v. Tabulated values of $\alpha(T)$ and $r(T)$ are then written as functions of v, smoothed and fitted with piecewise cubic splines.

References

1. *Welding Handbook*. 1991. Vol. 2, AWS, Miami, Fla., pp. 44–71.
2. Bracarense, A. Q., and Liu, S. 1993. Chemical composition variations in shielded metal arc welds. *Welding Journal* 72 (12): 549-s to 536-s.
3. Stern. I. L. 1948. Overheating of electrodes. *Welding Journal* 27(7): 522–526.
4. Ter Berg, J., and Larigaldie, A. 1952. Melting rate of covered electrodes. *Welding Journal* 32(5): 268-s to 271-s.
5. Bracarense, A. Q., and Liu, S. 1994. Control of covered electrodes heating by flux ingredients substitution. *Welding and Metal Fabrication* 62(5): 224–229.
6. Waszink, J. H., and Piena, M. J. 1985. Thermal processes in covered electrodes. *Welding Journal* 64(2): 37-s to 48-s.
7. Quinn, T. P., Madigan, R. B., and Siewert, T. A. 1994. An electrode extension model for gas metal arc welding. *Welding Journal* 73(10): 241-s to 248-s.
8. Jackson, C. E. 1973. Fluxes and slags in welding. *Welding Research Council Bulletin 190*.
9. Smith, J. M., and Van Ness, H. C. 1975. *Introduction to Chemical Engineering Thermodynamics*, pp. 116–132, McGraw-Hill.
10. Ray, H. S. 1993. *Kinetics of Metallurgical Reactions*. International Science Publisher, pp. 208–225.
11. Touloukian, Y. S. 1967. *The Elements*. Thermophysical properties of high temperature solid materials, Vol. 1. pp. 7–581. MacMillan Co., New York.
12. Touloukian, Y. S., Powell, R. W., Ho, C. Y., and Nicolaou, M. C. 1973. *Thermal diffusivity. Thermophysical Properties of Matter*, Vol. 10, pp. 2–82. IFI/Plenum, New York.
13. Touloukian, Y. S., and Buyco, E. H. 1970. *Specific heat. Thermophysical Properties of Matter*, Vol. 4, pp. 1–102. IFI/Plenum, New York.
14. Touloukian, Y. S., Powell, R. W., Ho, C. Y., and Klemens, P. G. 1970. *Thermal conductivity. Thermophysical Properties of Matter*, Vol. 1, pp. 9–109. IFI/Plenum, New York.
15. ASM International, 1983. Welding, brazing and soldering. *Metals Handbook*, Vol. 6, p. 81. ASM, Materials Park, Ohio.
16. Efron, B., and Tibshirani, R. J. 1993. *An Introduction to the Bootstrap*, Chapman and Hall, New York.
17. Brandi, S., Taniguchi, C., and Liu, S. 1991. Analysis of metal transfer in shielded metal arc welding. *Welding Journal* 70(10): 261-s to 270-s.
18. Krieth, F., and Black, W. Z. 1980. *Basic Heat Transfer*, pp. 255–320. Harper and Row, Cambridge, Mass.
19. Bracarense, A. Q. 1994. *Shielded Metal Arc Welding Electrode Heating Control by Flux Ingredients Substitution*. Ph.D. dissertation, pp. 149–152. Colorado School of Mines.
19. Crank, J. 1984. *Free and Moving Boundary Problems*, Oxford, Oxford University Press.
20. Forsythe, G. E., and Wasow, W. R. 1960. *Finite-Difference Methods for Partial Differential Equations*, pp. 68–71. John Wiley and Sons, New York.